Bonding, moment formation, and magnetic interactions in $Ca_{14}MnBi_{11}$ and $Ba_{14}MnBi_{11}$

D. Sánchez-Portal,[1,2] Richard M. Martin,[1] S. M. Kauzlarich,[3] and W. E. Pickett[4]

[1]*Department of Physics and Materials Research Laboratory, University of Illinois, Urbana, Illinois 61801*
[2]*Departamento de Física de Materiales and Donostia International Physics Center (DIPC), Facultad de Químicas, UPV/EHU, Apdo. 1072, E-20080 San Sebastián, Spain*
[3]*Department of Chemistry, University of California, Davis, California 95616*
[4]*Department of Physics, University of California, Davis, California 95616*

"14-1-11" phase compounds, based on magnetic Mn ions and typified by $Ca_{14}MnBi_{11}$ and $Ba_{14}MnBi_{11}$, show an unusual magnetic behavior, but the large number (104) of atoms in the primitive cell has precluded any previous full electronic structure study. Using an efficient, local-orbital-based method within the local-spin-density approximation to study the electronic structure, we find a gap between a bonding valence-band complex and an antibonding conduction-band continuum. The bonding bands lack one electron per formula unit of being filled, making them low carrier density p-type metals. The hole resides in the $MnBi_4$ tetrahedral unit, and partially compensates for the high-spin d^5 Mn moment, leaving a net spin near $4\mu_B$ that is consistent with experiment. These manganites are composed of two disjoint but interpenetrating "jungle gym" networks of spin-$\frac{4}{2}$ $MnBi_4^{9-}$ units with ferromagnetic interactions within the same network, and weaker couplings between the networks whose sign and magnitude is sensitive to materials parameters. $Ca_{14}MnBi_{11}$ is calculated to be ferromagnetic as observed, while for $Ba_{14}MnBi_{11}$ (which is antiferromagnetic) the ferromagnetic and antiferromagnetic states are calculated to be essentially degenerate. The band structure of the ferromagnetic states is very close to half metallic.

I. INTRODUCTION

Recently many new magnetic phenomena have been discovered, such as colossal magnetoresistance[1] (CMR), a new type of heavy fermion system[2] (LiV_2O_4), and spin Peierls ground states in magnetic insulators. Spin-glass behavior has been found and studied intensively in magnetic insulators without structural disorder.[3] A related aspect of complexity in crystalline magnets arises when magnetic ions are distributed regularly but interionic distances are large, ~ 1 nm. One example is the class of metallic rare earth (R) silicides $R_3Pd_{20}Si_6$, and the corresponding germanides, which present multiple ordering transitions with temperatures[4] in the range of a few K. Examples of dilute magnetic insulators are $Na_3M_2Li_3F_{12}$,[5] and the rare-earth phosphomolybdates[6] $RPO_4(MoO_3)_{12} \times 30H_2O$, which order below 1 K, and sometimes much below. A more well-known example is the heavy fermion superconductor UBe_{13}, which superconducts at 0.9 K and is near an antiferromagnetic instability.[7] These intriguing materials, with their complex exchange interactions transmitted through intermediate bonds, are examples of the continuing, perhaps even accelerating, growth and study of more complex compounds. The complexity may be structural in origin (many atomic sites of low symmetry in the unit cell), or it may be rooted in complex magnetic and electronic interactions (many different exchange couplings, perhaps competing and frustrating).

In this paper we present a first-principles density-functional study of the electronic properties of two representative compounds of the so-called "14-1-11" phases, which are a clear example of materials showing simultaneous complex atomic and magnetic structures. The 14-1-11 phases[8] typified by $Ca_{14}MnBi_{11}$, where Ca may be substituted for by

Sr or Ba and Bi can be substituted for by Sb or As,[9] comprise a rather difficult case of a magnetic system with a complex crystal structure. The structure will be described in detail below; however, with its four formula units (104 atoms) and nine inequivalent sites, and a magnetic ordering at 15–70 K indicating an exchange coupling of the order of 10 meV, this class presents a strenuous test for state-of-the-art electronic structure methods. Understanding the existence of such a structure is itself an interesting topic in solid state chemistry. It seems to be consistent with the simplified picture provided by the Zintl-Klemm-Bussmann[10] concept, which we will refer to as the Zintl concept. This picture represents a generalization of the octet rule for binary semiconductors and insulators, and invokes a charge balance between (nominally closed-shell) structural units which themselves may be covalently or ionically bonded complexes as well as simple ions. However, both of the compounds that we address in detail in this paper are metallic[11,12] in their magnetically ordered phases, whereas the Zintl arguments that have been applied to these compounds would be more appropriate if they were semiconducting. In fact, the magnetic ordering and the metallicity seem to be correlated in these materials, which would be broadly consistent with a Ruderman-Kittel-Kasuya-Yosida (RKKY)-type of model[13] for the origin of the magnetic interactions.

The two materials chosen for the present study are $Ca_{14}MnBi_{11}$, which is ferromagnetic (FM) with Curie temperature $T_C = 55$ K, and antiferromagnetic (AFM) $Ba_{14}MnBi_{11}$, with a Néel temperature $T_N = 15$ K. The observed magnetic moment of Mn and the ordering temperatures (several tens of K) give rise to several fundamental questions:

(1) What is the charge state of Mn, and how does it relate to structural stability and conduction behavior?

(2) Given that the Mn ions are magnetic, why is the or-

dering temperature of the order of 50 K when the distance between Mn ions is at least 10 Å?

(3) What is the bonding path that provides the magnetic coupling?

(4) How is the magnetic order coupled to the carriers in these compounds, some members of which show a colossal magnetoresistance near T_C?

The only previous theoretical work on the electronic structure of this class of compounds was done by Gallup, Fong, and Kauzlarich,[14] who considered a single-formula-unit simplification of semiconducting $Ca_{14}GaAs_{11}$. They concluded that the bonding in this compound is consistent with the Zintl concept of valence counting using covalently bonded subunits (discussed below). The greatest difference between this compound and those we study in this paper is the substitution of the sp metal atom Ga in the site of inversion symmetry with the transition-metal atom Mn. Ga is trivalent, whereas the metallicity of the Mn-based compounds indicates a different valence for Mn.

We conclude, in fact, that Mn is in a divalent state, with five $3d$ localized and magnetic electrons. This difference, trivalent Ga versus divalent Mn, leaves one unoccupied bonding orbital in the valence bands, giving a metallic behavior, as observed. The FM metal $Ca_{14}MnBi_{11}$ is close to a half-metallic filling[15] of the bands. Our results suggest that adding one additional electron per formula unit to the itinerant valence bands should lead to a semiconducting compound. Adding less than one more carrier could produce a half-metallic FM situation. The most direct way of doing so would be the replacement of a fraction of alkaline earth atoms with a trivalent atom, viz. Ca→Y. A less likely possibility would be Mn→Fe, if Fe would assume a trivalent, high-spin d^5 configuration. The alternative is that Fe would assume a d^6 configuration, and therefore also be divalent, and the system would remain metallic.

The current interpretation assigns a 3+ valence to the Mn atoms in these compounds.[16,17] This disagrees with our findings as stated above, but it seems a very reasonable assumption considering that the measured magnetic moment is very close to $4\mu_B$/Mn for this class of materials. However, Mn^{3+} also seems to imply a semiconducting character (viz. $Ca_{14}GaAs_{11}$), in contradiction to the experimental evidence. While the valence (or charge state) of an ion in a solid is a very useful concept, it does not necessarily represent an actual ionic charge; indeed, it is widely recognized that "ionic charge" is an ill-defined concept, particularly so for metals and narrow-gap semiconductors. Nevertheless, the "charge state" often continues to be meaningful, and the charge state of the Mn atom in these materials was deduced from measurements of the high-temperature magnetic susceptibility, which is indicative of moments of $\sim 4\mu_B$. This moment was assigned to Mn, arriving at a d^4 (trivalent) assignment. We find, however, that the density of states contains a peak, well below the Fermi energy, originating from five bands per formula unit (i.e., per Mn atom) which derive from Mn $3d$ states. This situation allows us to identify the Mn ion as having a d^5 configuration, consistent only with a divalent charge state. Nevertheless, the moment that we obtain is consistent with the experiment, being closer to $4\mu_B$ than to the

$5\mu_B$ expected from a simple d^5 configuration.

These two apparently contradictory observations are reconciled by the near-half-metallic band structure: the holes (one per Mn atom) left in the majority spin valence band reside in the Bi_4 tetrahedron that encapsulates the Mn ion. The effective $\sim 4\mu_B$ magnetic moment is still relatively well localized. As we will see below in more detail, both the experimental moment of $\sim 4\mu_B$ and our observation of an almost half-metallic band structure can already be anticipated from the electronic structure of the isolated $MnBi_4^{-n}$ tetrahedron, using the charge derived from applying the valence counting rules ($n=9$).

The paper is organized as follows. Sections II and III describe the crystal structure and the method of calculation, respectively. Magnetic energies and their interpretation in terms of exchange couplings are presented in Sec. IV, and Sec. V presents an analysis of the magnetization and its distribution along the unit cell. The density of states of crystalline $Ca_{14}MnBi_{11}$ and $Ba_{14}MnBi_{11}$ are analyzed in Sec. VI, followed by a discussion of charge transfers and their relation with the formal valences in Sec. VII. Section VIII is devoted to an examination of the electronic states near the Fermi level, along with their relation to the anisotropic nature of the magnetic couplings. In Sec. IX the main results for the solid are reinterpreted as simple consequences of the electronic structure of the isolated $MnBi_4$ charged clusters. A summary is presented in Sec. X.

II. CRYSTAL STRUCTURE AND ITS IMPLICATIONS

The structure of the alkaline-earth metal pnictide compounds $A_{14}MPn_{11}$, which we will call the AMPn structure, was experimentally determined, and described in detail by Kurotomo, Kauzlarich, and Webb.[11] In the present calculations we have used the coordinates given by these authors. $A_{14}MPn_{11}$ compounds have a body-center-tetragonal (space group $I4_1/acd$) unit cell with four formula units (104 atoms): $a=17.002$ Å and $c=22.422$ Å for $Ca_{14}MnBi_{11}$, and $a=18.633$ Å and $c=24.340$ Å for $Ba_{14}MnBi_{11}$.[11] The structure can be viewed as consisting of: interstitial alkaline earth atoms, isolated Bi ($Bi3^{18}$) atoms, distorted $MnBi_4$ ($Bi2$) tetrahedra, and Bi_3 ($Bi1$-$Bi4$-$Bi1$) linear units. The $MnBi_4$ tetrahedra are translated by $\frac{1}{2}$ along the c axis alternating with the Bi_3 anions, which are rotated by 90° with respect to each other, as shown in Fig. 1. The isolated Bi atoms are situated between the Bi_3 and $MnBi_4$ groups, along a screw axis which coincides with the c axis. All the Mn atoms in the unit cell are symmetry equivalent. The alkaline earth cations occupy four inequivalent sites, but the distinctions will not concern us.

The $MnBi_4$ tetrahedra are slightly flattened within the a-b plane, with the distortion increasing by $\sim 1°$ when Ca ion is substituted for by Ba (the inequivalent angles are 118.0° and 105.4° for the Ca compound). All bond lengths in the system also increase with this substitution, for which a and c increase by 9–10%, with a corresponding volume change of nearly 30%. The Mn-Bi bond distance, for example, increases from 2.814 Å (Ca) to 2.935 Å (Ba). The Bi-Bi bond length in the Bi_3 units also increases from 3.335 Å (Ca) to
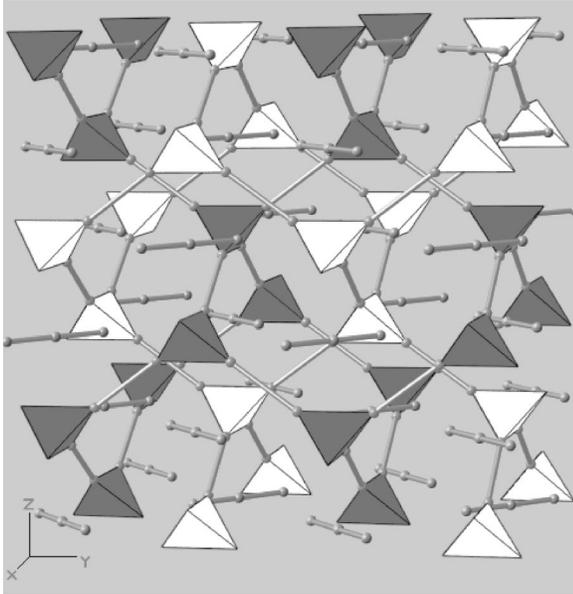
FIG. 1. One view of the crystal structure of $Ca_{14}MnBi_{11}$, emphasizing the two interpenetrating sublattices of $MnBi_4$ tetrahedra, one shown as white and the other one darker. The Bi_3 "sticks" are also shown; the Ca atoms and the isolated Bi atoms are not shown, for clarity.

3.498 Å (Ba),[11] indicating that both this unit and the $MnBi_4$ tetrahedra are substantially environment dependent.

There are four cations located close to the Bi2 atoms in the tetrahedron, with Bi-Ca distances in the range 3.2–3.3 Å, and 3.5–3.6 Å for Bi-Ba separations.[11] The Bi4 central atom in the Bi_3 unit is surrounded by four cations, while the terminal Bi1 atoms are coordinated with eight cations (Ca-Bi bonds of 3.2–3.4 Å, and Ba-Bi distances of 3.5–3.75 Å).[11]

As pointed out in Ref. 16, and which will prove to be important to understand the magnetic couplings, this crystalline structure can also be regarded as two interpenetrating networks formed by $MnBi_4$ tetrahedra. Each tetrahedron only belongs to one of these networks, and is linked to the four nearest $MnBi_4$ groups in the same network along the tetrahedral directions, i.e., through a Bi-Bi bond. This loose bond, with the Bi atoms 4.5–5 Å apart, is mediated by three cations (atoms $A1$, $A1'$, and $A3$ in Ref. 11), which are common nearest neighbors to both Bi (Bi2) atoms. Figure 2 shows a schematic representation of this connectivity on the (100) plane.

In contrast, the identification of the interaction pathway between $MnBi_4$ tetrahedra belonging to different networks is not so clear. Different paths can be envisioned, all involving several cations and at least one of the isolated Bi atoms (Bi3).

For compounds such as $A_{14}GaPn_{11}$, formal valence arguments and accumulated experience indicate that the electronic structure can be rationalized in terms of a model where each alkaline earth atom cedes two electrons ($14A^{2+}$), three of these valence electrons are collected by each isolated Pn atom ($4Pn^{3-}$), seven electrons can be transferred to the Pn_3 units leaving unoccupied the antibonding σ molecular state,[14] and the remaining electrons go to the tetrahedron
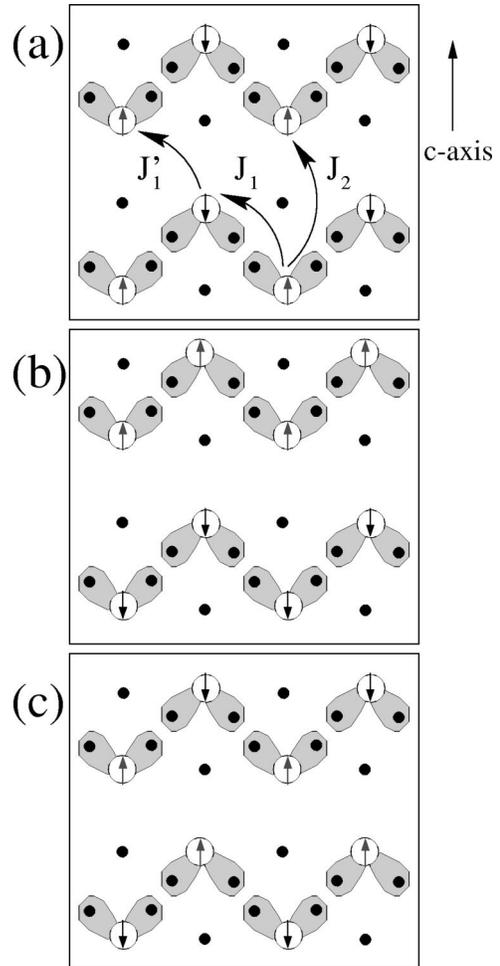
FIG. 2. Illustrations of the three inequivalent types of AFM order possible without enlarging the unit cell. A (100) plane is shown. The open circles with arrows indicate Mn with its spin direction, the filled dots indicate Bi sites, and the gray lobes indicate bonding patterns schematically. Some of the exchange constants are shown.

centered on the Ga atom which becomes $GaPn_4^{9-}$. Although these formal charges are quite large and should not be taken literally, such valence counting has proven to provide a very good description of the electronic structure of $Ca_{14}GaAs_{11}$.[14]

The metallic or semiconducting character of the $A_{14}MnBi_{11}$ materials therefore seems to depend in an essential way on the valence of the Mn atom. A trivalent Mn atom is isovalent with Ga and implies a semiconducting compound (which the $A_{14}MnBi_{11}$ compounds are not), while a divalent Mn ion will imply a metallic compound (as observed) but appears to violate formal charge neutrality. One of the main objectives of this paper is to resolve this conundrum.

III. METHOD OF CALCULATION

The calculations have been performed with the program SIESTA,[19–21] an optimized code which allows standard density-functional[22] calculations on systems with hundreds

TABLE I. Core radii (in a.u.) used for the generation of the pseudopotentials.

	Mn	Bi	Ca	Ba
r_s	2.00	2.20	3.20	3.50
r_p	2.20	2.90	3.30	4.00
r_d	1.90	2.90	3.00	3.50

of atoms. This method has been successfully applied to the study of the electronic and structural properties of many different materials,[23] including magnetic clusters.[24] The computational cost and memory requirements to build up the Hamiltonian matrix scale linearly with the size of the system, i.e., is of order N $[O(N)]$ where N is the number of atoms,[19,20] while for the evaluation of the density and energy one can choose between standard methods, or make use of the recently developed $O(N)$ techniques.[25] In this work we have used a standard diagonalization of the Hamiltonian because we are interested in the band structure and characteristics of specific states.

The basis set is a linear combination of pseudoatomic orbitals.[21,26,27] In the present calculations we have used a double-ζ polarized[21,28–30] basis set for all the atoms. A shell of d orbitals was also included for the Ba and Ca species. This amounts to 15 orbitals [two s, ten d, and a polarization (P) shell with $3p$ orbitals] for Mn, 13 orbitals (two s, six p, and five P d) for Bi, and ten orbitals (two s, five d, and three P p) in the case of Ca and Ba, making 1192 orbitals in total.

The core electrons are replaced by norm-conserving pseudopotentials[31] generated from the atomic configurations $[Ar]3d^5 4s^2$ for Mn, $[Hg]6p^{1.75}6d^{0.25}5f^{0.25}$ for Bi[32] and, $[Ar]4s^1$ and $[Xe]6s^1$ for Ca and Ba respectively. The core radii used in the generation of the pseudopotentials can be found in Table I. We apply the pseudopotentials using the fully separable formulation of Kleinman and Bylander.[33]

The calculations have been carried out in the local spin density approximation (LSDA),[34] and a partial-core correction for the nonlinear exchange correlation[35] has been included for all the species. This correction is especially important to obtain reliable moments in magnetic atoms, but some care has to be taken in choosing the pseudocore radius. We found that a pseudocore radius of 0.70 a.u. leads to very good results in comparison to all-electron calculations.[36]

IV. RESULTS FOR TOTAL ENERGIES AND MAGNETIC COUPLINGS

In this section we report on the relative stability of FM and AFM alignments of the Mn moments and the magnetic couplings deduced from the corresponding values of the total energy in both compounds. Since the calculations are already very large with the primitive crystallographic cell, we have not considered any magnetic alignments that would enlarge the cell. Even so, with four magnetic Mn atoms in the cell there are three distinct types of AFM alignments, shown in Fig. 2 in the (100) plane. The configurations are better explained in terms of two distinct ...-Mn-Bi-Bi-Mn-... "chains" in this plane: (i) in-phase AFM chains [Fig. 2(a)],

(ii) antialigned FM chains [Fig. 2(b)], and (iii) out-of-phase AFM chains [Fig. 2(c)]. Similar chains run out of this plane, and ultimately the various bonding chains form two interpenetrating three-dimensional networks, as described in Sec. II. Only four of the eight nearest Mn neighbors of a given Mn atom belong to the same network as the central one, and only in the configuration (i) (in-phase AFM chains) the eight neighbors are antiferromagnetically aligned.

From the figure it is clear that there are two distinct nearest neighbor interactions, labeled J_1 and J_1'. The second-neighbor interaction J_2 is also shown. We will obtain an estimate of these couplings assuming an effective spin coupling

$$H_{spin} = -\sum_t \sum_{\langle ij \rangle} J_{ij}^{(t)} S_i^z S_j^z, \qquad (1)$$

where $S_i^z = \pm 1$ represents a normalized spin variable. The index t labels the types of couplings, and $\langle ij \rangle$ denotes spin pairs of that type. Note that in some treatments, our J might correspond to JS^2 where S is the spin of the magnetic atom.

For both compounds we have calculated the energies for FM order and for the three AFM configurations described above. Of the AFM alignments, the antialignment of FM chains, as shown in Fig. 2(b), is always the one favored. Therefore, the minimum-energy AFM configuration occurs when one of the Mn networks is entirely spin-up, the other entirely spin-down.

Since the energy differences are quite small (as expected), it was necessary to study the convergence of the energies with respect to both the number of points (cutoff[37]) in the real-space grid, and the k-point mesh used to sample the Brillouin zone. Cutoffs up to 216 Ry for $Ca_{14}MnBi_{11}$ and 147 Ry for $Ba_{14}MnBi_{11}$ were used, with up to 12 k points in the irreducible Brillouin zone. The results shown in the following have been obtained with three inequivalent k points, and a cutoffs of 150 and 147 Ry for the Ca and Ba compounds, respectively. With these parameters the total energy is converged, for a given basis set, to 10 meV/Mn, while the energy differences between different configurations, which show a faster convergence, are converged to 5 meV/Mn.

The calculated total energy differences are presented in Table II. For $Ca_{14}MnBi_{11}$ the FM state is more stable by 25 ± 5 meV per Mn atom than the lowest energy AFM phase, in accord with the observation of ferromagnetism in this compound. In a simple nearest-neighbor Ising or Heisenberg modeling of the spin coupling, this energy would correspond to a FM exchange coupling of $J \sim 3$ meV. For $Ba_{14}MnBi_{11}$ the energy difference is much smaller, with the FM phase 4 ± 5 meV/Mn more stable, i.e., degenerate to within our accuracy. This compound is observed to be AFM, with $T_N = 15$ K, with the low ordering temperature reflecting smaller magnetic interactions than in $Ca_{14}MnBi_{11}$.

Table II also presents the exchange couplings of the effective spin Hamiltonian [Eq. (1)]. Each Mn atom has eight Mn first neighbors, four on the (100) planes and four on the (010) planes, at distances of 10.18 Å for the Ca compound (10.84 Å for $Ba_{14}MnBi_{11}$). Already from the energies in Table II, it is evident that two different first-neighbor cou-

TABLE II. Upper: energies of the three antiferromagnetic alignments pictured in Fig. 2 relative to the ferromagnetic alignment. The type of AFM order in $Ba_{14}MnBi_{11}$ [type (a), (b), or (c), or other, is not established experimentally]. Numerical uncertainties are expected to be $\sim \pm 5$ meV. Lower: Exchange couplings for a short-range Ising model determined from the total-energy differences. The couplings correspond to those pictured in Fig. 2. J_{2+3} are the value of the couplings if second and third neighbors would enter in the energy expression via a single exchange constant (see the text).

Energy (meV)	$Ca_{14}MnBi_{11}$	$Ba_{14}MnBi_{11}$
AFM(a)–FM	59	12
AFM(b)–FM	25	4
AFM(c)–FM	52	13
Experiment	FM	AFM
Exchange constants (K)	$Ca_{14}MnBi_{11}$	$Ba_{14}MnBi_{11}$
J_1	63 ± 5	15 ± 5
J_1'	23 ± 5	2 ± 5
J_2	27 ± 10	7 ± 10
J_{2+3}	9 ± 3	2 ± 3
T_C, mean field	130 ± 20 K	28 ± 20 K
T_C, experiment	$T_C = 55$ K	$T_N = 15$ K

plings need to be included. In fact, if just one exchange constant were to be used in a model with only first-neighbor interactions, the energies of configurations (b) and (c) in Fig. 2 should be identical. Physically, the need of two constants is easily understood as a consequence of the presence of two Mn networks: stronger interactions can be expected within the same network (J_1) than between atoms in different networks (J_1'). This is clearly confirmed in Table II, where J_1 is shown to be much lager than J_1' for both compounds.

There are two second neighbors located at 11.21 Å (12.17 Å) along the c axis. The four third neighbors can be found 12.02 Å (13.18 Å) away, along the $\langle 100 \rangle$ and equivalent directions. In the crystallographic cell these last atoms are equivalent to the second neighbors, yet located at somewhat larger distances due to the tetragonal distortion of the cell. Further neighbors are at more than 17 Å for both compounds, and their interaction constants are expected to be much smaller. With the calculated energy differences we cannot make independent estimations of the second (J_2) and third (J_3) nearest-neighbor couplings. At this point, we can choose to restrict the interactions up to second neighbors, and obtain a value for J_2. Another possibility is to consider second and third neighbors as entering into Eq. (1) at the same footing, i.e., through an *averaged* coupling constant [$J_{2+3} = (2J_2 + 4J_3)/6$]. The values for these exchange constants are also listed in Table II.

V. MAGNITUDE AND DISTRIBUTION OF THE MAGNETIC MOMENT

In this section we study the distribution of the magnetic moment in the unit cell with the help of the Mulliken population analysis.[38] It must be recognized that the populations

TABLE III. Population and moments of the Mn d shell, and magnetic moments of Mn atoms and $MnBi_4$ tetrahedra as obtained from a Mulliken population analysis for the FM $Ca_{14}MnBi_{11}$, and $Ba_{14}MnBi_{11}$. $\mu_{A_{14}MnBi_{11}}$ stands for the net magnetic moment per formula unit, while μ_{eff}^{expt} is the effective moment per Mn atom as obtained from measurements of the high-temperature magnetic susceptibility.

	$Ca_{14}MnBi_{11}$	$Ba_{14}MnBi_{11}$
$Q_d^{\uparrow}$	4.67	4.74
$Q_d^{\downarrow}$	0.51	0.42
μ_d	4.16	4.32
μ_{Mn}	4.45	4.62
μ_{MnBi_4}	4.22	4.35
$\mu_{A_{14}MnBi_{11}}$	4.25	4.40
μ_{eff}^{expt}	4.8	4.8

obtained using a Mulliken analysis suffer, like those obtained via all similar techniques, from an inherent arbitrariness: both the charge density and the total charge are observables of the system, but their partition into different atomiclike contributions cannot be uniquely defined. Accordingly, Mulliken population trends and differences are more meaningful than their absolute values, and their use is fairly common. In this way we obtain information about the effective valence state and magnetic moment of the Mn atoms, the polarization of the surrounding atoms, and the degree of localization of the total magnetic moment.

The magnetic moments on the Mn atoms for the FM compounds, as obtained from the difference between the Mulliken populations of the majority- and minority-spin densities, are shown in Table III. They are found to be nearly independent of the type of magnetic order, and differ by 4%: $4.45\mu_B$ for $Ca_{14}MnBi_{11}$, and $4.62\mu_B$ for $Ba_{14}MnBi_{11}$. The parts of the moment attributable to the $3d$ shell are $4.16\mu_B$ and $4.32\mu_B$, respectively, with about $0.1\mu_B$ and $0.2\mu_B$ induced in the $4s$ and $4p$ states in each compound. The spin-up population (Table III) of the Mn $3d$ orbitals approaches five electrons, indicative of a d^5 configuration. Several factors can contribute to a reduction of the $3d$ population, the most important being the hybridization with the $6p$ states of the neighboring Bi atoms. The identification of the configuration of Mn as $3d^5$ will be also confirmed from a detailed analysis of the electronic band structure (see Sec. VI B), providing further support to our picture of a divalent Mn atom.

The total moments per formula unit of the FM state are calculated to be (see Table III) $4.25\mu_B$ for $Ca_{14}MnBi_{11}$ and $4.40\mu_B$ for $Ba_{14}MnBi_{11}$, which become $17\mu_B$ and $17.6\mu_B$ per cell, respectively. With all the majority d states occupied, each Mn atom should contribute with a magnetic moment of $+5\mu_B$ ($+20\mu_B$ in the unit cell). However, an analysis of the contributions to the d bands indicates that this moment, although still mostly localized in Mn, is somewhat spread out to the neighboring Bi atoms (Bi2) due to the considerable hybridization between the Mn $3d$ states and the $6p$ states of Bi. Therefore, it is more safely pictured as associated with

the five atoms in the MnBi$_4$ tetrahedra, rather than with the Mn atoms alone.

A reverse polarization of $(2.4–3)\mu_B[(0.6–0.75)\mu_B/$ MnBi$_4$ unit] must be present to recover the calculated moment. From the data in Table III it is clear that this back polarization is also concentrated in the MnBi$_4$ tetrahedra, whose magnetic moment almost recovers the total value per formula unit. Part of this is due to the occupation, through hybridization, of the minority-spin Mn d orbitals. The remainder is mostly divided among the Bi2 atoms, which have a magnetic moment of $\sim -0.06\mu_B$ per Bi atom, the largest in the cell after Mn. This moment is quite modest, but it is in fact built up from two much larger contributions that tend to cancel each other: $\sim +0.20\mu_B$ coming from their participation in the majority Mn $3d$ bands (as previously commented), and a $\sim -0.26\mu_B$ component coming from the polarized Bi $6p$ bands responsible for the reverse polarization. The amount of spin polarization spread around the rest of the cell is negligible ($\sim 0.001\mu_B$ per Bi or A atom on average). Only the isolated Bi atoms (Bi3), and the alkaline-earth atoms (A1 and A3) connecting the MnBi$_4$ tetrahedra present a small polarization of $\sim -0.03\mu_B$ and $\sim +0.02\mu_B$, respectively.

An analysis of the Mulliken populations of all the studied AFM orders, for both Ca and Ba compounds, indicates a very similar picture: the calculated moment per formula unit has to be assigned to the MnBi$_4$ tetrahedra, being neither fully localized in the Mn ion nor spread over the whole unit cell. This moment, of $\sim 4\mu_B$, is built up from two distinct contributions: a $\sim 5\mu_B$ moment coming from the fully occupied majority spin $3d$ shell of Mn, and a $\sim -1\mu_B$ reverse polarization coming from the $6p$ states of the four Bi atoms in the MnBi$_4$ complex. The MnBi$_4$ tetrahedra are therefore the *magnetic units* in these compounds.

Experimentally, an effective moment (μ_{eff}) of $4.8\mu_B$ has been obtained for both compounds from the high-temperature susceptibility.[11] In fact, for all the related compounds A_{14}MnPn$_{11}$, where Bi is substituted for by Sb or As, and the cation sites are occupied by Ca, Sr, or Ba atoms, μ_{eff} is always found within the range $(4.8–5.4)\mu_B$.[9,11] For Yb$_{14}$MnBi$_{11}$ and Yb$_{14}$MnSb$_{11}$ (Refs. 16, 17) μ_{eff} is also measured to be $4.9\mu_B$. This has been interpreted, using the standard form for the Curie constant, $\mu_{eff}^2 = g^2 J(J+1)\mu_B^2$ where J is the total effective angular moment and g is the Landé g factor,[39] as a signature of the presence of localized $\sim 4\mu_B$ moments in all these compounds. This seems to be in good agreement with our calculated magnetic moment per formula unit (i.e., per MnBi$_4$ tetrahedron). However, all previous works assigned these magnetic moments solely to the Mn atoms, leading to the conclusion that Mn is in a 3+ valence state with four unpaired d electrons, which is in contradiction by our findings.

A better quantity to compare with our calculation of the magnetic moment is the experimental saturation moment, which is the value of the ordered moment parallel to the applied field $\langle M_z \rangle$. The initial work on hysteresis loops for powder samples,[9,11] observed saturation moments of $(2.5–3)\mu_B/$Mn, which are $\sim 30\%$ smaller than both the es-
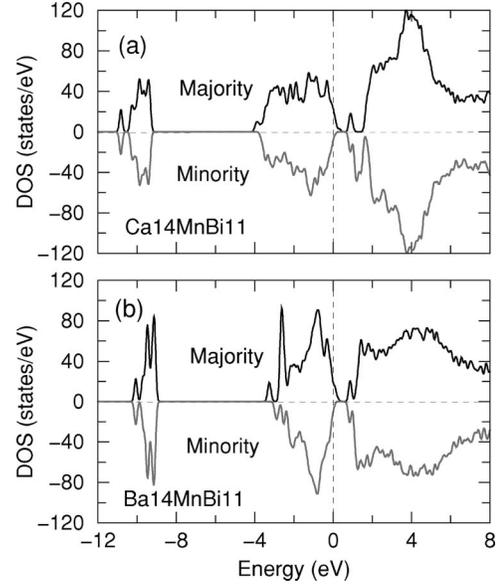
FIG. 3. Total densities of states per unit cell for (a) ferromagnetically aligned Ca$_{14}$MnBi$_{11}$ and, (b) Ba$_{14}$MnBi$_{11}$. The energies refer to the Fermi level.

timations based on the measured Curie constants and our calculated total moments. The polarization of the itinerant valence electrons was invoked in those works to explain this discrepancy between the measured saturation moments and the fitted μ_{eff}. However, more recent measurements using single crystals[40,17] indicated that the saturation moment is close to $4\mu_B/$Mn, in better agreement with our calculations.

VI. DECOMPOSITION OF THE ELECTRONIC SPECTRUM

Besides the character of the band structure near the Fermi energy, which will be discussed in detail in a separate section, the general features of the electronic structure and ordering of the levels are the same for both FM and AFM orders, and very similar for Ca and Ba compounds. Therefore we will concentrate here on the FM order.

A. Total density of states, general structure

With five valence electrons for Bi, two for Ca, and seven for Mn, and four formula units per cell, the occupied valence bands of these compounds must accommodate 360 electrons, or roughly 180 occupied bands of each spin. The total density of states (DOS) of FM Ca$_{14}$MnBi$_{11}$ and Ba$_{14}$MnBi$_{11}$ are shown in Figs. 3(a) and 3(b), respectively, which also reveal some general features. These plots have been obtained using three inequivalent k points and a Gaussian broadening of 0.1 eV. Tests indicate that using more complete k sampling (up to 12 inequivalent k points) produces almost identical results. The occupied valence bands are $4–4.5$ eV wide and nearly filled. A "gap" of ~ 1 eV separates the valence complex from a continuous spectrum of unoccupied states coming mainly from the Ca-Bi hybridization. Within the gap, 0.5 eV above the top of the valence band, we find four narrow (0.2 eV) bands. In the minority-spin DOS, near the top of the gap

for $Ca_{14}MnBi_{11}$, and confused with the onset of the conduction band in $Ba_{14}MnBi_{11}$, we can also find a peak that contains the unoccupied Mn $3d$ bands.

The band complexes below the gap consist of 182 bands of each spin for AFM states, for which the spin directions are equivalent. For FM order there are 192 majority band and 172 minority bands, as the majority bands contain 20 more bands (for the five occupied $3d$ electrons of the four Mn atoms) than the minority bands. The total number of bands in the valence complex is consequently the same for FM and AFM states: four electrons lacking for these compounds to become semiconductors. The 172 bands not associated with the d states of Mn have mainly a Bi character. 44 of them, located approximately 9 eV below the Fermi energy, are due the Bi $6s$ states. The remaining 128, which form the uppermost valence-band complex, can be classified as Bi $6p$ bands, exhibiting some degree of hybridization with Mn and Ca/Ba states. From the 44 Bi atoms present in the unit cell we could expect to have 132 Bi $6p$ bands, however. The four Bi $6p$ bands left out of the valence complex form the, already mentioned, narrow peak in the middle of the gap. These bands correspond to very localized states associated with the Bi_3 chains (see below).

The DOS at the Fermi energy (E_F) is higher for the majority spin (Fig. 3), and both compounds are very close to half metallic, with the minority bands almost fully occupied (as discussed later). From the specific heat Siemens *et al.*[12] obtained the Fermi level DOS $N(E_F) = 1.7 \pm 0.7$ states/ eV atom for $Ba_{14}MnBi_{11}$, and 1.6 ± 0.1 states/eV atom for the similar compound $Sr_{14}MnBi_{11}$. These are quite large values, comparable to the DOS of d band metals. However, Siemens *et al.* pointed out that contributions to the specific heat coming from the nuclear hyperfine splitting, not taken into account in their analysis, could obscure their results, leading to large apparent values of the electronic DOS. In fact, our estimations of the DOS at E_F are much smaller: $N(E_F) = 0.3$ states/eV atom for both Ca and Ba compounds with FM order. For AFM order, $N(E_F) = 0.40–0.46$ states/eV atom depending on the specific AFM alignment. These values can be compared with the average DOS in the valence-band complex; leaving aside the Mn bands, we have 256 bands for both spin orientations distributed over a range of ~ 4 eV, leading to an average $\langle N(E) \rangle = 0.6$ states/ eV atom.

B. Mn character

Because of the magnetic moment on the Mn atom, we begin our discussion of the electronic bonding with the Mn d states. In all the cases we have considered, the simple characterization is that the majority d states are filled and the minority states are empty, with an exchange splitting between them of ~ 4 eV. Accordingly, the Mn atom can be described as having a $3d^5$ configuration or, alternatively, a $2+$ valence. The $MnBi_4$ tetrahedron is compressed along the a-b plane, and only the d_{xz} and d_{yz} states are degenerate, so the crystal-field results in four distinct d levels. The crystal-field splitting is negligible, however. In $Ca_{14}MnBi_{11}$ ($Ba_{14}MnBi_{11}$), shown in Fig. 4, the majority d states lie in a
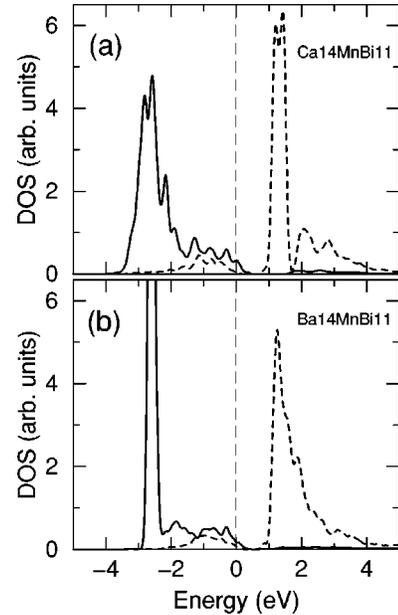
FIG. 4. Densities of states projected into the Mn d states in (a) $Ca_{14}MnBi_{11}$ and, (b) $Ba_{14}MnBi_{11}$. The Fermi level defines the zero of energy. Solid lines denote the majority-spin DOS, and dashed lines the minority-spin DOS. The exchange splitting is ~ 4 eV in each case.

single peak centered 2.7 eV below E_F with a width of roughly 1 eV (respectively 0.4 eV). The d states do hybridize with all states above this peak (with mainly Bi $6p$ character) to the gap just above E_F. The minority states are unoccupied and are concentrated in a peak 1.3 eV above E_F. This unoccupied peak is narrow in $Ca_{14}MnBi_{11}$ (0.6 eV), and lies within the gap (also see Fig. 9). In $Ba_{14}MnBi_{11}$ it is much broader (at least 1 eV) meeting the bottom of the conduction band, and exhibiting a higher degree of hybridization with the conduction states.

C. Bi character

The spin-averaged DOS projected into the different types of Bi atoms in the unit cell can be found in Fig. 5. The Bi $6s$ bands lie 9–10 eV below the Fermi level, and have a negligible hybridization with states of different characters. The Bi $6p$ states make up a large component of the valence bands, exhibiting hybridization with both Mn and alkaline-earth states, and hence are crucial in the bonding and in the magnetic coupling. The valence bands are 4 eV wide in $Ba_{14}MnBi_{11}$, and slightly (5%) wider in the smaller volume $Ca_{14}MnBi_{11}$ compound. There is a "gap" of ~ 1 eV between the valence and conduction bands, *except* that a very narrow set of unoccupied bands lies within this gap. Although in Fig. 5 we have neglected the small effects due to the induced exchange splitting, it should be kept in mind that the polarization of the Bi $6p$ states near E_F is crucial to understanding the magnitude and distribution of the magnetic moment.

The complications are still considerable, since there are four distinct Bi sites. The Bi2 sites correspond to the distorted $MnBi_4$ tetrahedron, the Bi_3 linear chain is formed by a central Bi4 atom bonded to two Bi1 atoms, and there are also
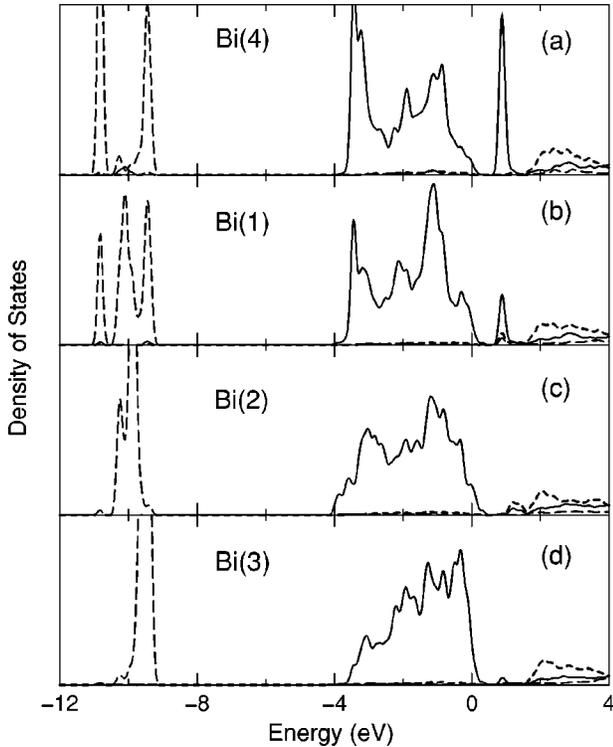
FIG. 5. Densities of states projected into the s (long dashed lines at lower energies), p (solid line), and d (dashed lines at higher energies) symmetry orbitals of the Bi1, Bi2, Bi3, and Bi4 sites in ferromagnetically aligned $Ca_{14}MnBi_{11}$. The differences occur primarily in the gap region 0–2 eV, and are discussed in the text. Spin-averaged spectra have been plotted; only the polarization on the Bi2 site ($\sim -0.06\mu_B$) is appreciable.

FIG. 6. Contour plot in the (001) plane of the density of the antibonding $\sigma^\star$ states localized in the Bi_3 chains of FM $Ca_{14}MnBi_{11}$. These four bands are located within the gap, around 1 eV above the Fermi energy. The contours begin at 3×10^{-4} $e/Bohr^3$, and increase by steps of 6×10^{-4} $e/Bohr^3$ (seven and 14 electrons per unit cell respectively). The positions of the Mn and Bi atoms in the plane are indicated schematically.

four isolated Bi3 atoms. The first thing that is evident from the Bi spectra in Fig. 5 is that there is not a great deal of difference in the densities of states of the four Bi sites, indicating that their charges are not very different. The Bi1-Bi4-Bi1 linear unit has only a small (but nonzero) DOS at E_F, whereas both the Bi2 bonded to the Mn and the "isolated" Bi3 site have much larger fractions of the Fermi-level DOS. In the case of the Bi2 atoms this DOS is almost entirely due to the majority spin contribution.

The unoccupied "gap states," one state, and therefore one band for each Bi_3 unit (four in the unit cell) are associated with the Bi1 and Bi4 atoms only, with no appreciable spin polarization. Since they lie in the gap and have a dispersion of only 0.2 eV, these states are quite localized. Figure 6 shows contour plots of their density in a plane containing the Bi1-Bi4-Bi1 sites. Their shape, with nodes in the bond region between Bi1 and Bi4 atoms, and the fact that (see Fig. 5) they have a larger weight in the central Bi4 atom, reveal them as antibonding σ molecular orbitals. The presence of these $\sigma^\star$ states and the negligible population of the $5d$ states of the Bi4 atom, which rules out the possibility of a dsp^3 hybridization, confirm the description of the Bi_3^{7-} anion as a hypervalent "three center, four electron" bonded structure. This type of bonding was already predicted for As_3 in $Ca_{14}GaAs_{11}$ by Gallup et al.,[14] who applied first-principles calculations to a simplified model (30-atom unit cell) of this compound. The conduction bands contain the rest of the Bi $6p$ spectral weight along with Bi $5d$, Ca or Ba s, and Mn $3s$, $3p$, and minority $3d$ contributions.

D. Ca/Ba character

The formal valence picture suggests considering the Ca and Ba atoms as dipositive ions. This picture should not be taken too literally, as we find some s, p, and d alkaline-earth contributions to the DOS in the valence-band region (figure not shown). The Ca/Ba d DOS peaks lie 4 eV above E_F, whereas the s and p contributions are spread over a large region from ~ -3 eV through and above the d bands, with rather little structure in their distribution.

VII. CHARGE TRANSFER AND FORMAL VALENCE

Now we address the question of whether the formal valence that the Zintl picture associated with the different groups of atoms provides a reasonable description of our results. The formal valences are Ca^{2+}/Ba^{2+}, isolated Bi^{3-}, Bi_3^{7-} linear chains, and $MnBi_4^{9-}$ tetrahedra. These latter two are very large charges and, as can be expected, the Mulliken populations are much smaller, although still indicative of large charge transfers. For example for $Ca_{14}MnBi_{11}$ we obtain $Ca^{0.8+}$, $MnBi_4^{3.7-}$, $Bi_3^{2.8-}$, and $Bi^{1.2-}$. The main reason for this difference between formal and Mulliken charges can be traced back to the fact that, while there is not a single state with pure or main Ca/Ba character, most of the states in the valence band exhibit some small hybridization with the orbitals of the alkaline-earth atoms, specially those at the top of the valence band with the d states of Ca/Ba. In fact, the s population of the alkaline-earth ions (the only orbital that would be included in a simplified description of these atoms) is only 0.4 electrons for both Ca and Ba compounds, pictur-

FM $Ba_{14}MnBi_{11}$
Deformation density plot
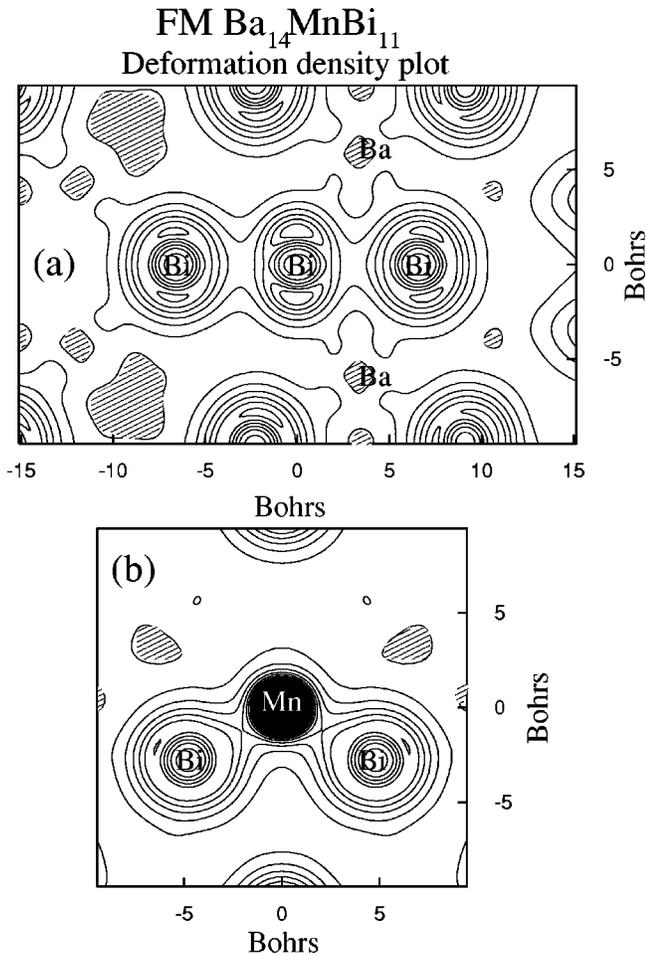
FIG. 7. (a) Contour plot of the deformation density of ferromagnetically aligned $Ba_{14}MnBi_{11}$ in a (110) plane, illustrating the Bi_3 unit bonding (top panel). The bottom panel (b) shows the (100) plane through the $MnBi_4$ tetrahedron, indicating that the charge "deformation" is rather spherical around the atoms and is therefore primarily charge transfer. Only the region of increased charge is shown, with contours beginning at zero and increasing by $0.03e/Å^3$. The position of the atoms in the planes is indicated by their chemical symbol. The shaded areas correspond to regions with defect of charge.

ing them as $Ca(Ba)^{1.6+}$. Furthermore, Ca/Ba components are generally very small for each individual eigenstate of the solid, and formally they can be safely considered as dipositive.

Figure 7 shows the contour plots of the deformation density (the difference between the self-consistent charge density and that obtained from the sum of spherical neutral atom contributions) in different planes for FM $Ba_{14}MnBi_{11}$. Two things can be observed: (i) there is a great deal of charge transfer to the Bi atoms from the Ca/Ba atoms, which are always surrounded by a region showing a depletion of charge; and (ii) the deformation density is quite featureless and spherical around the Bi atoms, indicating that indeed the ionic charge transfer is the main mechanism involved.

We now consider the polyatomic anions. The situation of Bi_3 is specially clear. Two antibonding molecular states (one per spin) remain unoccupied, and the valence states are al-

most completely occupied up to the gap, with a very small contribution to the Fermi level DOS (see Figs. 5 and 6). All these data together identify the Bi_3 unit as having a formal valence of 7. The weight of the gap peaks in Fig. 5 suggest that less charge is transferred to the central Bi4 than to the Bi1 sites, which is confirmed by the Mulliken analysis (around $0.3|e|$ less). This completely agrees with the "three-center, four-electrons" model of bonding proposed for the Bi_3 unit.[14]

We now discuss the cases of the $MnBi_4$ units and the isolated Bi3 ions. On the one hand, a formal charge of 3 would correspond to closed-shell Bi3 anions, with a negligible contribution to the DOS at E_F. On the other hand, considering the $2+$ effective valence (d^5) of the Mn atom, the $MnBi_4$ group would be formally able to accept up to ten electrons. This implies that a $MnBi_4^{9-}$ tetrahedron would be lacking one electron to be closed shell. This agrees with our analysis of the electronic structure (Sec. VI A), which indicates that these compounds lack four electron per unit cell (i.e., one electron per $MnBi_4$ group) to become semiconductors. Furthermore, taking into account the calculated reverse polarization of the Bi2 sites, the hole associated to each $MnBi_4^{9-}$ tetrahedron should be expected to be aligned with the atomic moment of the corresponding Mn. This is confirmed by the data presented in Fig. 8, where a plot of the density associated to the holes for AFM $Ca_{14}MnBi_{11}$ [alignment type (a) of those shown in Fig. 2] in the (100) plane is shown. This plane contains Mn atoms, some of the Bi2 atoms bonded to them, and Bi4 sites. We can verify how the holes, while not exactly confined to the tetrahedra, are fairly localized in the tetrahedra: the spin-up holes in those tetrahedra where the atomic moment of Mn points in the up direction, and conversely for spin-down holes. It is worthwhile to mention here that a similar electronic structure, i.e., a $3d^5$ Mn plus a weakly bound polarized hole, was also proposed by several authors for the Mn_{Ga} centers in GaAs in the high dilution limit.[41] An obvious consequence of this polarization of the valence band holes is the (close to) half-metallic character of the band structure of the FM compounds, which will be examined in detail in Sec. VIII. Hence we can conclude that the identification of a valence of 9 for the $MnBi_4$ unit and a valence of 3 for the Bi3 ions are meaningful, and from the point of view of a general picture our results are consistent with counting of formal charges.

VIII. ELECTRONIC STATES NEAR THE FERMI LEVEL

A. Character of the states

For simplicity we will first discuss the case of the AFM order. Figure 9 shows the band structure for AFM $Ca_{14}MnBi_{11}$ [alignment type (b) of those shown in Fig. 2]. There are two bands unfilled below the gap, and hence there are four electrons less (i.e., one per formula unit) than required to make this compound a semiconductor. The figure shows in detail the region of the "gap" between bonding and extended conduction states. For each spin orientation this gap contains two groups of bands corresponding to very localized states: one very narrow group of four bands coming
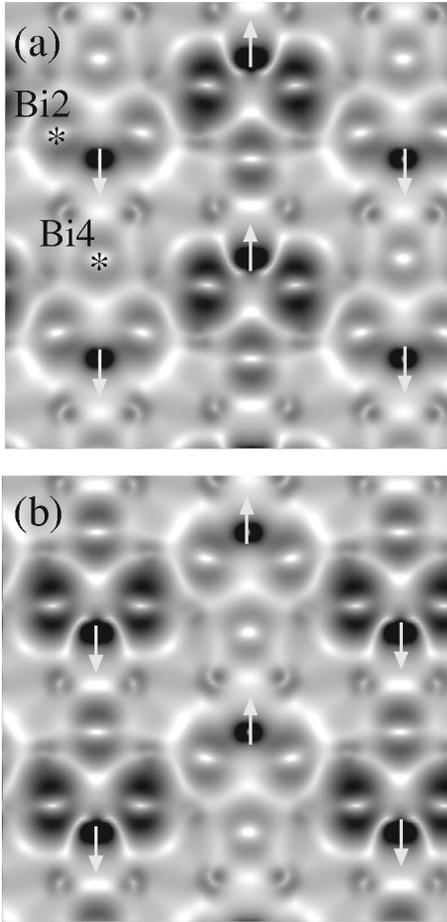
FIG. 8. Gray scale plot in a (100) plane of the (pseudo)charge density associated to the unoccupied states below the gap (holes) in AFM $Ca_{14}MnBi_{11}$. Panel (a) shows the spin-up holes, and panel (b) the spin-down holes. The arrows schematically indicate the positions of the Mn atoms and the orientations of their atomic magnetic moments. The positions of one of the Bi2 and Bi4 atoms are also indicated. We have used a logarithmic scale which saturates to black at $10^{-3}e/Bohr^3$ and to white at $10^{-5.3}e/Bohr^3$ (respectively, 22 and 0.1 electrons per unit cell).

from the antibonding states of the Bi_3 chains in the energy range 0.85–1.05 eV, and ten unoccupied $3d$ Mn bands in the range 1.2–1.6 eV, the last ones almost degenerate with the beginning of the continuum of conduction states. The energy position of these groups of bands is very similar for AFM and FM states, but while the Bi_3 bands do not show any spin polarization, for FM order the 20 unoccupied Mn $3d$ bands only occur in the minority band structure.

B. Half-metallicity of FM compounds

The bands for both FM $Ca_{14}MnBi_{11}$ and $Ba_{14}MnBi_{11}$ near E_F, along several symmetry directions, are shown in Fig. 10. Except for details (which affect the Fermi-surface shape and therefore might become important) the bands are similar, and we discuss their common characteristics. The band structure is very close to half-metallicity. The minority bands are occupied except for a Γ-centered pocket that contains only a
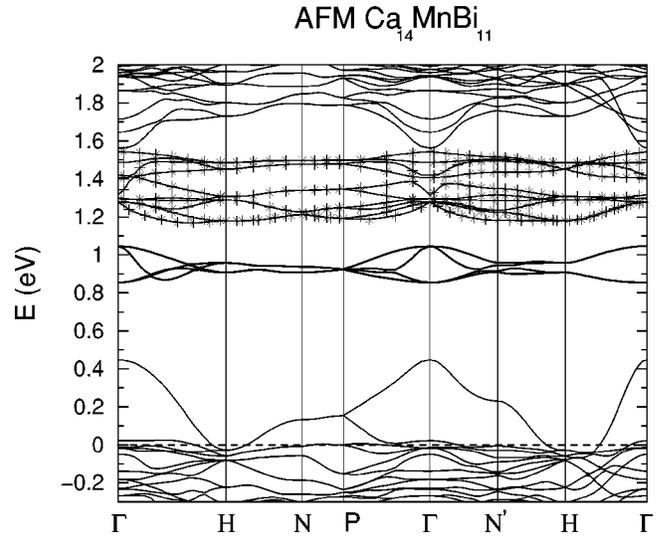
FIG. 9. Band plots along primary symmetry directions for antiferromagnetically aligned $Ca_{14}MnBi_{11}$. The narrow bands at 0.8–1.1 eV arise from the antibonding $\sigma^\star$ states localized in the Bi_3 chains. Those marked with stars are formed by the unoccupied d states of Mn. The energies refer to the Fermi level.

fraction of a hole (around 50%). The rest of the four holes correspond to the majority bands, which have several partially occupied bands: five in $Ca_{14}MnBi_{11}$ and four in $Ba_{14}MnBi_{11}$.

The almost half-metallic band structure is especially interesting in light of the reported colossal magnetoresistance in the related compound $Eu_{13.97}Gd_{0.03}MnSb_{11}$.[42] The CMR system $La_{1-x}D_xMnO_3$, with $D=$ Ca, Sr, or Ba, and $x\sim\frac{1}{3}$, are believed to be half-metallic or close to it.[1] $Eu_{13.97}Gd_{0.03}MnSb_{11}$ represents a case in which a compound, $Eu_{14}MnSb_{11}$, that is isovalent with the ones studied here is doped with additional carriers ($Eu^{2+}\rightarrow Gd^{3+}$), which will drive it toward half-metallicity.
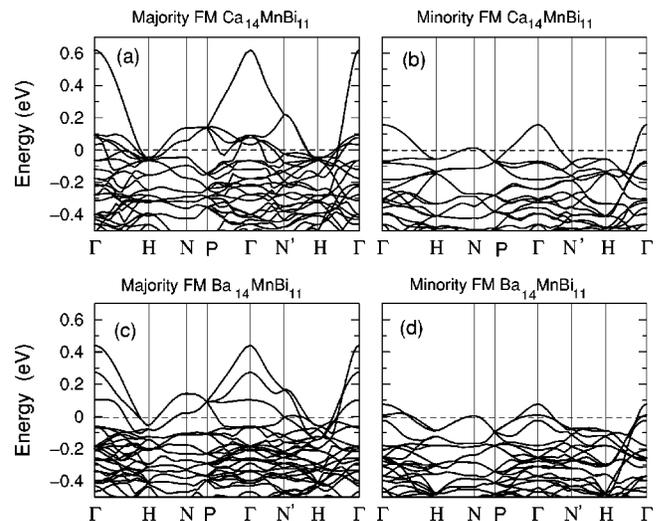
FIG. 10. Band plots in the vicinity of the Fermi level along primary symmetry directions for ferromagnetically aligned $Ba_{14}MnBi_{11}$ and $Ca_{14}MnBi_{11}$. The symmetry points correspond to the tetragonal bcc unit cell. The energies refer to the Fermi level.
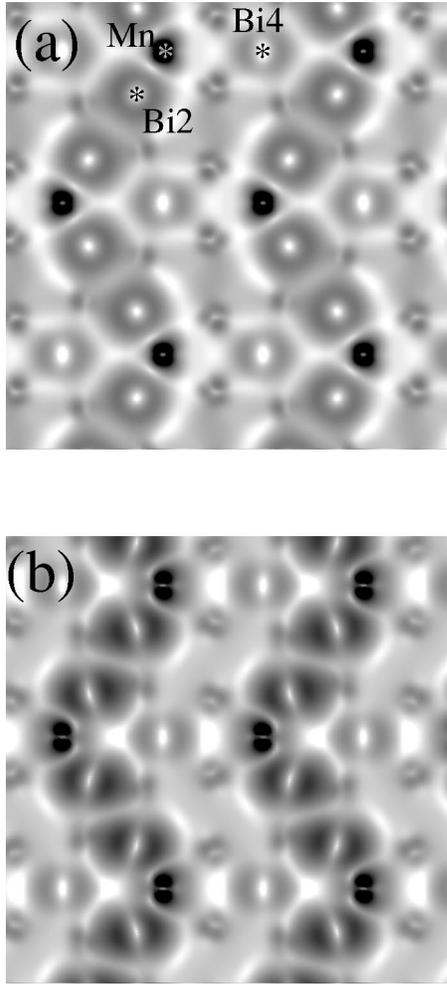
FIG. 11. Gray scale plot in a (100) plane of the (pseudo)charge density near E_F in FM $Ca_{14}MnBi_{11}$. The top panel (a) shows occupied states, and the bottom panel (b) holes. The positions of one of the Bi2, Bi4, and Mn atoms in the plane are schematically indicated. Note the bonding chains coupling Mn atoms (darkest spots) formed by the two intervening Bi2 atoms. We have used a logarithmic scale which saturates to black at $10^{-2.8} e/Bohr^3$ and to white at $10^{-5.3} e/Bohr^3$ (35 and 0.1 electrons per unit cell respectively).

C. Magnetic couplings

An RKKY model for the magnetic interaction is the simplest assumption to make in a dilute magnetic metal, and, in the absence of other information, that is what has been used so far in the interpretation of magnetic coupling in these 14-1-11 magnets.[16] Our identification of near-neighbor couplings (Table II) invalidates a spherical RKKY model, where the coupling strength depends only on distance. This conclusion is supported by Fig. 11, which shows a gray scale plot of the (pseudo-)charge density from states near E_F in $Ca_{14}MnBi_{11}$ in a (100) plane containing -Mn-Bi2-Bi2-Mn- bonding chains. In this figure, panel (a) contains the density from states in the range from E_F-0.5 eV to E_F. Panel (b) contains the charge density from the unoccupied states between E_F and the gap (holes). Both panels clearly show that the density associated to the states near E_F concentrates along the -Mn-Bi2-Bi2-Mn- chains, making them the most

likely conduit for the exchange coupling between Mn atoms. The occupied states, panel (a), shows direct charge peaks along this bonding chain, although the states may be predominantly antibonding. Panel (b) also indicates the density along this chain, and is apparently more antibonding, since the charge maxima centered on the Bi2 sites do not point toward the neighboring Mn atom. However, this has to be taken with some caution since, as already discussed in Sec. II, other atoms may intervene in the bonding between neighboring $MnBi_4$ units. In particular, three Ca/Ba common nearest-neighbors of those Bi2 atoms in neighboring connected tetrahedra, which are not contained in the (100) plane shown. In fact, the charge maxima in Fig. 11(b) seem to point from the Bi2 atoms to some of those alkaline-earth ions located $\sim \pm 0.7$ Å over the plane.

The general picture of the magnetic couplings that arises from our calculations is the following: Mn atoms are divided between two different networks (defined by the -Mn-Bi2-Bi2-Mn- bonding chains); the nearest-neighbor coupling within the same network is the strongest and always FM; the couplings among Mn atoms belonging to different networks are much smaller and may be AFM, explaining the experimental AFM ground state of $Ba_{14}MnBi_{11}$. In particular, the presence of two internally FM coupled networks is consistent with the observation that, although it suffers an AFM transition, the Curie temperature obtained for $Ba_{14}MnBi_{11}$ from the fitting of the high-temperature magnetic susceptibility is positive.[11] Therefore, although we have failed to predict the antiferromagnetism of $Ba_{14}MnBi_{11}$, we expect that the magnetic alignment in this compound must be quite similar to the most stable of the AFM orders discussed in this paper [Fig. 2(b)], i.e., one network is entirely spin-up, and the other entirely spin-down.

It may be worthwhile to point out here that the electronic structure of the 14-1-11 manganites shares several common features with that of diluted magnetic semiconductors (DMS's) (Ref. 43), like $Ga_{1-x}Mn_xAs$: both systems are p-type conductors; the valence-band electrons exhibit an antiferromagnetic coupling with the Mn atomic spin, and the band structure of the FM phases is close to half-metallic; Mn is tetrahedrally coordinated with group-V atoms, with a similar interpretation of the electronic structure of the Mn centers in the highly diluted limit (small x),[41] i.e., a 2+ Mn ion ($3d^5$) plus a weakly localized hole. Both types of systems exhibit magnetic order in spite of the large separation between magnetic ions, $Ga_{1-x}Mn_xAs$ (Ref. 44) being a ferromagnet with a Curie temperature exceeding 100 K for the optimum doping range.[45] Based on all these similarities, we consider it likely that the mechanism leading to ferromagnetism in DMS's is similar to the mechanism that drives most of the 14-1-11 manganites to a FM ground state, and that produces strong FM interactions between those Mn atoms belonging to the same network of $MnBi_4$ tetrahedra in both Ca and Ba compounds. Unfortunately, while there is a widespread agreement on the hole mediated origin of ferromagnetism in $Ga_{1-x}Mn_xAs$ and related compounds, the detailed mechanism is still a matter of some controversy.[46]

The origin of the AFM ground state of $Ba_{14}MnBi_{11}$, i.e., the antiparallel alignment of the internally FM coupled net-
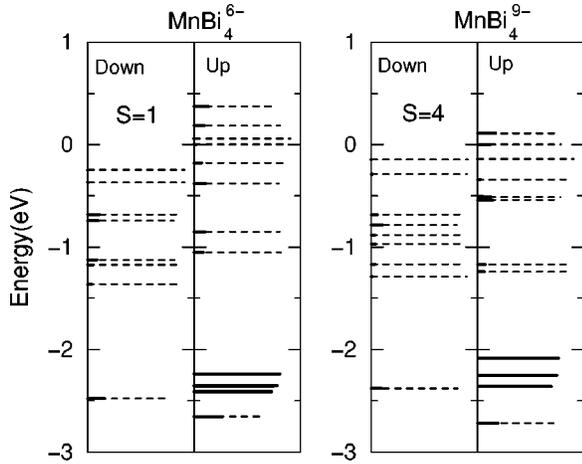
FIG. 12. Energies of the molecular orbitals of the $MnBi_4^{9-}$ and $MnBi_4^{6-}$ tetrahedral clusters. The zero of energy is located at the highest occupied molecular orbital. The cluster geometry was fixed to that of the $MnBi_4$ tetrahedron in crystalline $Ba_{14}MnBi_{11}$. See the text for notation.

works, is then probably related to the presence in this compound of (nonspherical) RKKY-type AFM interactions between Mn magnetic moments in different networks. The superexchange mechanism can also play a role, although, in our estimation, a less important one. However, the very small energy difference between the FM and AFM orders in $Ba_{14}MnBi_{11}$ constitutes an important difficulty in order to identify the relevant mechanisms that determine the sign of the "internetwork" magnetic interactions.

IX. DISCUSSION: STUDY OF CHARGED MnBi₄ CLUSTERS

The results of the previous sections point out that, rather than the Mn ions, the $MnBi_4$ tetrahedra should be considered as *magnetic units* in these compounds. The amount of charge transferred to the $MnBi_4$, in combination with the effective valence of the Mn atom, also plays a crucial role in understanding the magnetic moment, the conduction properties, and the interplay between them. For this reason we devote a separated section to the study of electronic structure of free standing charged $MnBi_4$ tetrahedral clusters and how these results translate into implications for the solid.

Figure 12 shows some of the energy levels of clusters with a total net charge of $-9|e|$ (nominal for the $MnBi_4$ group in the $A_{14}MnBi_{11}$ compounds), and a smaller charge of $-6|e|$. The geometry of the cluster was kept fixed to that of a $MnBi_4$ tetrahedron in crystalline $Ba_{14}MnBi_{11}$. Due to the use of periodic boundary conditions, it was necessary to assume a uniform neutralizing background in the calculations. The horizontal scale represents the projection of each molecular orbital (MO) into the different atomic species. Solid and thinner dashed lines correspond to Mn and Bi_4 contributions, respectively (which sum to unity). Different degeneracies of the levels have not been taken into account in making the figure. Only the group of levels close to the highest occupied molecular orbital (HOMO) is shown, corresponding

TABLE IV. Total magnetic moment S (μ_B), as a function of the net charge Q_e ($|e|$) and total number of valence electrons N_e, for $MnPbBi_3$, $MnBi_4$, and, $MnBi_3Po$ tetrahedral clusters with a central Mn atom. The cluster geometry was kept to that of the $MnBi_4$ tetrahedra in crystalline $Ba_{14}MnBi_{11}$.

Q_e	$MnPbBi_3^{Q_e-}$		$MnBi_4^{Q_e-}$		$MnBi_3Po^{Q_e-}$	
	N_e	S	N_e	S	N_e	S
-6	32	0	33	1	34	2
-7	33	1	34	2	35	3
-8	34	2	35	3	36	4
-9	35	3	36	4	37	5
-10	36	4	37	5	–	–
-11	37	5	–	–	–	–

to MO's mainly due to the Mn $3d$ and Bi $6p$ states. Therefore, in the range of energies shown in Fig. 12, there are 12 MO's for both spin orientations, and five additional MO's for the majority spin (only three levels are seen in Fig. 12 due to the degeneracies) with main character in the Mn $3d$ states, which corroborates the d^5 configuration of the Mn atom also in the case of the free-standing $MnBi_4$ clusters. Only one of the Bi $6p$ MO's has a larger binding energy than the Mn $3d$ states. This MO has a clear bonding configuration, with a p orbital from each Bi atom pointing in phase toward the central Mn, and includes some hybridization with the s symmetry orbitals of Mn. Above the energy levels shown in Fig. 12 there is a "gap" of ~ 2 eV (~ 3 eV) for the minority (majority) spin, and well below the HOMO (~ -9 eV) four MO's coming from the Bi $6s$ states can be found.

The most striking fact of the electronic structure presented in Fig. 12 is the *half-metallic* character it suggests: the minority-spin valence states are all occupied for both clusters, lying at least 0.2 eV below the HOMO. This situation holds for a large range of net charging of the $MnBi_4$ clusters, showing the robustness of the half-metallicity. The most probable origin of this polarization of the Bi states is the Pauli exclusion principle: the majority-spin MO's have to be orthogonal to the localized Mn $3d$ orbitals, and the corresponding increase in kinetic energy pushes these levels to higher energies than those of the minority-spin states. As a result, the Bi $6p$ states are polarized oppositely to the Mn $3d$ moment.

As a consequence of the half-metallic electronic structure, the total spin of the tetrahedral $MnBi_4$ clusters depends on the total number of valence electrons, as shown in Table IV. Taking into account the d^5 configuration obtained for the Mn atom, the MO's due to the $6p$ Bi states can still accommodate up to ten extra electrons. In that case, with a net charge of $-10|e|$, both majority and minority states are fully occupied and the magnetic moment of the cluster is equal to that of the Mn $3d$ shell ($5\mu_B$). If the net charge of the cluster is then reduced, the holes are always created in the majority spin MO's and, as a consequence, the total spin of the cluster is reduced. In particular, the formal charge of the $MnBi_4$ group in the manganites studied in this paper is $-9|e|$ (see Sec. VII), which leaves one unoccupied majority-spin state. Therefore, consistent with the electronic structure of the

TABLE V. Population of the Mn d shell and magnetic moments of different groups of atoms, as obtained from a Mulliken population analysis for FM $Ba_{14}MnBi_{11}$, and the compounds obtained by substituting a Bi atom in one of the $MnBi_4$ tetrahedra by a Pb atom and a Po atom, respectively. In all cases the structure of the $Ba_{14}MnBi_{11}$ was maintained. The data correspond to the substituted ($MnBi_3X$) groups, while those in brackets correspond the remaining $MnBi_4$ tetrahedra.

| | $Ba_{56}Mn_4Bi_{43}X$ | | |
	$X = Pb$	$X = Bi$	$X = Po$
Q_d	5.14 (5.15)	5.15	5.16 (5.15)
μ_d	4.24 (4.33)	4.32	4.34 (4.32)
μ_{Mn}	4.56 (4.63)	4.62	4.66 (4.62)
μ_{MnBi_3X}	3.73 (4.39)	4.35	4.52 (4.32)
$\mu_{unit\ cell}$	16.98	17.59	17.04

clusters and the formal valence, we can expect a magnetic moment of $\sim 4\mu_B$ on each $MnBi_4^{9-}$ tetrahedron, as obtained in our calculations for the solids. The data in Table IV also show that, if the charge transfer to the Mn tetrahedra is lower than nine electrons, even a larger reduction of the magnetic moment could be expected. The robustness of the dependence of the total spin on the number of electrons is also shown by substituting one of the Bi atoms by Pb, which provides one electron less, and by a Po atom, which provides one electron more than Bi to the cluster valence population.

Since the rest of the atomic groups in the unit cell are formally closed shell, we can expect the main properties of the crystal to arise from $MnBi_4$ clusters, at least as far as the interaction between $MnBi_4^{9-}$ units is weak enough in the solid. With such a simplified model we can already anticipate the following properties.

(i) The presence of a polarized hole localized in each $MnBi_4$ tetrahedron.

(ii) As a consequence of the reverse polarization of the valence-band holes, the magnetic moment should be reduced considerably from the Mn^{2+} value to near $4\mu_B$.

(iii) The FM order should exhibit a half-metallic band structure with approximately four unoccupied majority-spin bands (one for each Mn atom in the unit cell).

(iv) The hopping of these holes between neighboring tetrahedra should be the main mechanism of electric transport.

These results are in fact corroborated by the calculations for the solids presented in the previous sections, that take into account the full interconnectedness of the lattice. In addition, we have performed calculations for some fictitious materials that provide further support to the idea that an argumentation based on the MO's of the isolated clusters is still meaningful for the crystal. In one case we have substituted a Bi atom with Pb in one of the $MnBi_4$ groups of the unit cell of $Ba_{14}MnBi_{11}$. According to Table IV the magnetic moment of the resulting $MnPbBi_3^{9-}$ tetrahedron should decrease to $3\mu_B$ from the $4\mu_B$ of the pure Bi cluster. In Table V we can see that, in the solid, this substitution is in fact accompanied by a decrease of both the total (by $0.61\mu_B$) and the local magnetic moment, which becomes $3.73\mu_B$ for the tetrahedron where the substitution has been performed while

is almost unchanged for the rest of the tetrahedra ($4.39\mu_B$). The case of the Po substitution is a little bit more complicated. The magnetic moment of $MnBi_3Po^{9-}$ should increase to $5\mu_B$. This is again reflected in the results for the solid, but in this case the observed change is more modest, $4.52\mu_B$ versus $4.32\mu_B$ (see Table V). This different behavior is related to two different effects. In the first place, the Po substitution adds one electron to the tetrahedron which is probably accompanied by a delocalization of the associated MO's (Wannier functions in the solid); thus the picture solely based on the electronic structure of the isolated clusters becomes less accurate. Another effect comes from the fact that the band structure of $Ba_{14}MnBi_{11}$, while very close to half-metallic, is not totally half-metallic. With the addition of one electron the half-metallicity is reached, forcing the total magnetic moment to have integer values, which consequently diminishes it from $17.59\mu_B$ to $17\mu_B$ with the Po substitution. As expected, all the changes of the magnetic moment observed upon chemical substitution occur without much modification of either the charge or the moment associated to the Mn atom, or its d shell.

X. CONCLUSIONS

In this paper we have presented and analyzed the results of first-principles, full-unit-cell, LSDA calculations of $Ca_{14}MnBi_{11}$ and $Ba_{14}MnBi_{11}$. The general agreement between our results and the available experimental information supports a microscopic framework within which to understand these complex materials, which show the simultaneous presence of localized Mn magnetic moments and metallicity. We also provide evidence of additional properties, not yet corroborated by measurements, such as near half-metallicity of the FM manganites. We summarize our main conclusions as follows.

(i) Electron counting based on the Zintl picture, which visualizes these materials as an ionically bound collection of dipositive alkaline earth ions and negatively charged ions and covalently bonded polyatomic anions ($MnBi_4^{9-}$, B_3^{7-}, and Bi^{3-}), is a good starting point for the description of the electronic structure of these compounds, as suggested by Gallup et al.[14]

(ii) The Mn ions should be regarded as divalent Mn^{2+}, rather than the original picture that considers a d^4 configuration ($3+$ valence) for the Mn ion. Charge balance is maintained by the introduction of one hole into the Bi $6p$ states in the $MnBi_4$ tetrahedron; a heuristic connection $Ga^{3+}(Bi_4)^{12-} \longleftrightarrow Mn^{2+}(Bi_4)^{11-}$ can be drawn, which also relates the charge states in the tetrahedron to the insulating or conducting character of the solid. The hole in the Bi_4 tetrahedron can hop to neighboring $MnBi_4$ units, accounting for the (hole) conduction in $Ca_{14}MnBi_{11}$ and $Ba_{14}MnBi_{11}$.

(iii) In spite of the majority Mn $3d$ states being fully occupied, the experimental magnetic moment of $\sim 4\mu_B$ per formula unit (i.e., per Mn atom) is recovered in our calculations, since the hole in the Bi_4 tetrahedron is parallel to the Mn moment (the unpaired electron is antiparallel).

(iv) The FM compounds are close to half-metallic, with the minority bands almost completely occupied.

(v) The AMPn crystal structure introduces its own peculiar magnetic coupling. The MnBi$_4$ tetrahedra (the *magnetic units* of these compounds) are distributed in two disjoint interpenetrating three dimensional networks. Magnetic coupling is ferromagnetic within each network, and AFM order arises if there are AFM interactions between tetrahedra from different networks. These anisotropic magnetic couplings cannot be understood within a traditional, isotropic RKKY scheme.

(vi) Our calculations also provide some insight into the puzzle of how the transition temperatures can be as high as 70 K for this family of compounds when the Mn-Mn are more than 10 Å apart. One point is that the Mn-Mn distance is not the meaningful parameter, rather the relevant parameter is the Bi2-Bi2 distance which determines the hopping along the -Mn-Bi2-Bi2-Mn- chains.

(vii) We speculate that full three-dimensional ordering is enhanced by the comparatively strong FM coupling within each network, analogously to the situation in layered cuprates such as La$_2$CuO$_4$ which order magnetically above room temperature in spite of very weak interlayer exchange coupling.[49]

Our new picture of Mn in the AMPn structure should impact the interpretation of the valence fluctuation behavior of Yb$_{14}$ZnSb$_{11}$, where indications are that both Yb^{2+} and Yb^{3+} ions are present.[50] Dipositive Zn destroys the electron count that would result in semiconducting behavior (viz. Ca$_{14}$Ga^{3+}As$_{11}$). The system accommodates by drawing an electron from the Yb ions, which is possible because of the near degeneracy of the Yb^{2+} and Yb^{3+} configurations. However, it may also be possible to draw an electron from the $5p$

cluster orbitals of some of the Sb$_4$ tetrahedra, as is done in every Bi$_4$ tetrahedron in Ca$_{14}$MnBi$_{11}$ and Ba$_{14}$MnBi$_{11}$, with an accompanying unbalanced spin. Further study will be required to develop a consistent picture of this fluctuating valence system.

Our description also gives insight into the interplay between the conduction and magnetic properties, and may play a crucial role in the CMR behavior observed in some of the 14-1-11 manganites. In particular, it provides a simple picture of the pressure induced ferromagnetic transition observed in Sr$_{14}$MnAs$_{11}$,[51] which seems to be accompanied by a semiconductor-metal transition, and was previously interpreted as signature of a RKKY-type magnetic interaction. Compressing the AMPn structure causes an increase in the interaction between the MnBi$_4$ units, with the corresponding increase of the hopping probability of the localized valence-band holes. These holes are simultaneously responsible of the conduction process and vehicles of the exchange interaction between Mn atoms and, therefore, a decrease in the resistivity of these systems is necessarily accompanied by stronger magnetic interactions.

[1] See *Physics of Manganites*, edited by T. A. Kaplan and S. D. Mahanti (Kluwer/Plenum, New York, 1999).

[2] S. Kondo, D.C. Johnston, and L.L. Miller, Phys. Rev. B **59**, 2609 (1999).

[3] J.E. Greedan, J. Mater. Chem. **11**, 37 (2001); P. Schiffer and A.P. Ramirez, Comments Condens. Matter Phys. **18**, 21 (1996); A.P. Ramirez, Annu. Rev. Mater. Sci. **24**, 453 (1994).

[4] J. Kitagawa, N. Takeda, and M. Ishikawa, J. Alloys Compd. **256**, 48 (1997); J. Kitagawa, N. Takeda, F. Sakai, and M. Ishikawa, J. Phys. Soc. Jpn. **68**, 3413 (1999).

[5] S. Chamberlain and L.R. Corruccini, J. Phys. Chem. Solids **58**, 899 (1997).

[6] L.R. Corruccini, J.T. van der Noorda, S.J. White, and H. Hope, Physica B **240**, 43 (1997).

[7] B. Batlogg D. Bishop, B. Golding, C. M. Varma, Z. Fisk, J. L. Smith, and H. R. Ott, Phys. Rev. Lett. **55**, 1319 (1985); A. P. Ramirez, B. Batlogg, E. Bucher, and A. S. Cooper, *ibid.* **57**, 1072 (1986); R. H. Heffner, J. L. Smith, J. O. Willis, P. Birrer, C. Baines, F. N. Gygax, B. Hitti, E. Lippelt, H. R. Ott, A. Schenck, E. A. Knetsch, J. A. Mydosh, and D. E. MacLaughlin, *ibid.* **65**, 2816 (1990); F. Kromer, R. Helfrich, M. Lang, F. Steglich, C. Langhammer, A. Bach, T. Michels, J. S. Kim, and G. R. Stewart, *ibid.* **81**, 4476 (1998).

[8] *Chemistry, Structure, and Bonding of Zintl Phases and Ions*, ed-ited by S. Kauzlarich (VCH, New York, 1996), Ch. 6.

[9] A. Rehr, T.Y. Kuromoto, S.M. Kauzlarich, J. Del Castillo, and D.J. Webb, Chem. Mater. **6**, 93 (1994).

[10] E. Zintl, Angew. Chem. **52**, 1 (1939); W. Klemm, Proc. Chem. Soc. London **1958**, 329; E. Bussmann, Z. Anorg. Allg. Chem. **313**, 90 (1961).

[11] T.Y. Kuromoto, S.M. Kauzlarich, and D.J. Webb, Chem. Mater. **4**, 435 (1992). The unit cell used by crystallographers is twice as large.

[12] D.P. Siemens, J. Del Castillo, W. Potter, D.J. Webb, T.Y. Kuromoto, and S.M. Kauzlarich, Solid State Commun. **84**, 1029 (1992).

[13] M.A. Ruderman and C. Kittel, Phys. Rev. **96**, 99 (1954); K. Yosida, *ibid.* **106**, 893 (1957); T. Kasuya, Prog. Theor. Phys. **45**, 58 (1956).

[14] R.F. Gallup, C.Y. Fong, and S.M. Kauzlarich, Inorg. Chem. **31**, 115 (1992).

[15] W.E. Pickett and J.S. Moodera, Phys. Today **54** (1), 39 (2001).

[16] S. M. Kauzlarich, A. C. Payne, and D. J. Webb, in *Magneto-Science: From Molecules to Materials*, edited by J. S. Miller and M. Drillon (Wiley, New York, 1999).

[17] I.R. Fisher, T.A. Wiener, S.L. Bud'ko, P.C. Canfield, J.Y. Chan, and S.M. Kauzlarich, Phys. Rev. B **59**, 13 829 (1999).

[18] Here we will follow the nomenclature used in Ref. 11 to denote

the inequivalent sites of the different species.

[19] P. Ordejón, E. Artacho, and J.M. Soler, Phys. Rev. B **53**, R10 441 (1996); *Materials Theory, Simulations, and Parallel Algorithms*, edited by E. Kaxiras, J. Joannopoulos, P. Vashishta, and R. K. Kalia, MRS Symposia Proceedings No. 408 (Materials Research Society, Pittsburgh, 1996), p. 85.

[20] D. Sánchez-Portal, P. Ordejón, E. Artacho, and J.M. Soler, Int. J. Quantum Chem. **65**, 453 (1997).

[21] E. Artacho, D. Sánchez-Portal, P. Ordejón, A. García, and J.M. Soler, Phys. Status Solidi B **215**, 809 (1999).

[22] W. Kohn and L.J. Sham, Phys. Rev. **140**, A1133 (1965).

[23] A short review of the applications of the SIESTA method can be found in P. Ordejón, Phys. Status Solidi B **217**, 335 (2000).

[24] M. Calleja, C. Rey, M.M.G. Alemany, L.J. Gallego, P. Ordejón, D. Sánchez-Portal, E. Artacho, and J.M. Soler, Phys. Rev. B **60**, 2020 (1999); J. Izquierdo, A. Vega, L.C. Balbás, D. Sánchez-Portal, J. Junquera, E. Artacho, J.M. Soler, and P. Ordejón, *ibid.* **61**, 13 639 (2000).

[25] P. Ordejón, D.A. Drabold, M.P. Grumbach, and R.M. Martin, Phys. Rev. B **48**, 14 646 (1993); F. Mauri, G. Galli, and R. Car, *ibid.* **47**, 9973 (1993).

[26] O.F. Sankey and D.J. Niklewski, Phys. Rev. B **40**, 3979 (1989). A study of the performance of these basis sets can be found in, D. Sánchez-Portal, E. Artacho, and J.M. Soler, J. Phys.: Condens. Matter **8**, 3859 (1996).

[27] In order to limit the range of the orbitals, they are slightly excited by an *energy shift*, and truncated at the resulting radial node. By using the same energy shift for all the orbitals in the calculation we can avoid the appearance of unphysical population changes and charge transfers. In this work we have used an energy shift of 0.25 eV. The corresponding radii are 4.86 and 6.40 a.u. for the s and p orbitals of Bi, 6.56 and 3.88 a.u. for the s and d orbitals of Mn, 6.08 and 5.23 a.u. for those of Ca, and 7.08 and 6.68 a.u. in the case of Ba.

[28] J. Junquera, O. Paz, D. Sánchez-Portal, and E. Artacho, Phys. Rev. B **64**, 235111 (2001).

[29] The double-ζ orbitals are constructed in the spirit of the *split-valence* [see, for example, S. Huzinaga *et al.*, *Gaussian Basis Sets for Molecular Calculations* (Elsevier, Amsterdam, 1984)]. The split-off function reproduces the tail of the original orbital beyond some radius, matching to a smooth $r^l(a-br^2)$ form toward the nucleus. The matching radius was chosen, in this case, so that the split orbital carries a 25% of the norm of the original one.

[30] Polarization functions are constructed perturbatively from the original orbitals, and have the same confinement radius.

[31] N. Troullier and J.L. Martins, Phys. Rev. B **43**, 1993 (1991).

[32] G.B. Bachelet, D.R. Hamann, and M. Schluter, Phys. Rev. B **26**, 4199 (1982).

[33] L. Kleinman and D.M. Bylander, Phys. Rev. Lett. **48**, 1425 (1982).

[34] D.M. Ceperley and B.J. Alder, Phys. Rev. Lett. **45**, 566 (1980), as parametrized by J.P. Perdew and Y. Wang, Phys. Rev. B **45**, 13 244 (1992).

[35] S.G. Louie, S. Froyen, and M.L. Cohen, Phys. Rev. B **26**, 1738 (1982).

[36] The Mn pseudopotentials were tested by reproducing all-electron results for Mn_2 VAl calculated by R. Weht and W.E. Pickett, Phys. Rev. B **60**, 13 006 (1999).

[37] These cutoffs indicate the fineness of the real-space grid where the electronic density is projected in order to calculate the exchange correlation, and part of the self-consistent Hartree contributions to the total energy and Hamiltonian matrix. The energy cutoff is the maximum energy of a plane wave that can be represented using such a grid.

[38] R.S. Mulliken, J. Chem. Phys. **23**, 1841 (1955).

[39] N. W. Ashcroft and N. D. Mermin, *Solid State Physics* (Holt-Saunders, Philadelphia, 1976).

[40] D.J. Webb, R. Cohen, P. Klavins, R.N. Shelton, J.Y. Chan, and S.M. Kauzlarich, J. Appl. Phys. **83**, 7192 (1998).

[41] J. Schneider, U. Kaufmann, W. Wilkening, M. Baeumler, and F. Köhl, Phys. Rev. Lett. **59**, 240 (1987); M. Linnarsson, E. Janzén, B. Monemar, M. Kleverman, and A. Thilderkvist, Phys. Rev. B **55**, 6938 (1997).

[42] J.Y. Chan, S.M. Kauzlarich, P. Klavins, J.-Z. Liu, R.N. Shelton, and D.J. Webb, Phys. Rev. B **61**, 459 (2000).

[43] See for example, T. Dietl, H. Ohno, F. Matsukura, J. Cibert, and D. Ferrand, Science **287**, 1019 (2000), and references therein.

[44] H. Ohno, A. Shen, F. Matsukura, A. Oiwa, A. Endo, S. Katsumoto, and Y. Iye, Appl. Phys. Lett. **69**, 363 (1996).

[45] F. Matsukura, H. Ohno, A. Shen, and Y. Sugawara, Phys. Rev. B **57**, R2037 (1998).

[46] Dietl and co-workers (Refs. 43 and 47) studied the problem using a Zener model of ferromagnetism, and obtained a good agreement with experiment. Another proposal, based on the so-called ''double exchange'' mechanism, was made by Akai (Ref. 48).

[47] T. Dietl, H. Ohno, and F. Matsukura, Phys. Rev. B **63**, 195205 (2001).

[48] H. Akai, Phys. Rev. Lett. **81**, 3002 (1998)

[49] S. Chakravarty, B.I. Halperin, and D.R. Nelson, Phys. Rev. Lett. **60**, 1057 (1988).

[50] I.R. Fisher, S.L. Bud'ko, C. Song, P.C. Canfield, T.C. Ozawa, and S.M. Kauzlarich, Phys. Rev. Lett. **85**, 1120 (2000).

[51] J. Del Castillo, D.J. Webb, S.M. Kauzlarich, and T.Y. Kuromoto, Phys. Rev. B **47**, 4849 (1993).